Support information

High Er Doping in CeO_2 via Lanthanide Contraction Boosts Oxygen Vacancy Formation and Ammonia Decomposition

Ji-Zhou Yang[1#], Zheng Li[1#], Jun-Kang Guo[1*], Chong-Qi Chen[2], Chun-Jie Yuan, Li-Long Jiang[2], Shuang-Feng Yin[1,3*]

[1]College of Chemistry and Chemical Engineering, State Key Laboratory of Chemo and Biosensing, Advanced Catalytic Engineering Research Center of the Ministry of Education, Hunan University, Changsha 410082, P. R. China

[2]National Engineering Research Center of Chemical Fertilizer Catalyst, School of Chemical Engineering, Fuzhou University, Fuzhou 350002, Fujian, P. R. China

[3]College of Chemistry and Chemical Engineering, Central South University of Forestry and Technology, Changsha 410004, P. R. China

[#]These authors contributed equally to this work.

Corresponding Authors**:**

Jun-Kang Guo, E-mail: jkguo@hnu.edu.cn;

Shuang-Feng Yin, E-mail: sf_yin@hnu.edu.cn

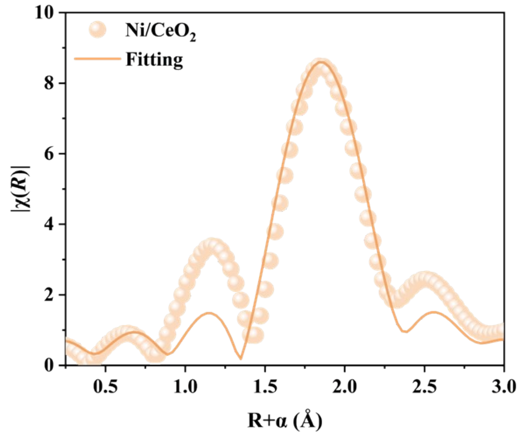

Figure S1. Ce-O K-edge XANES spectra of Ni/CeO_2.

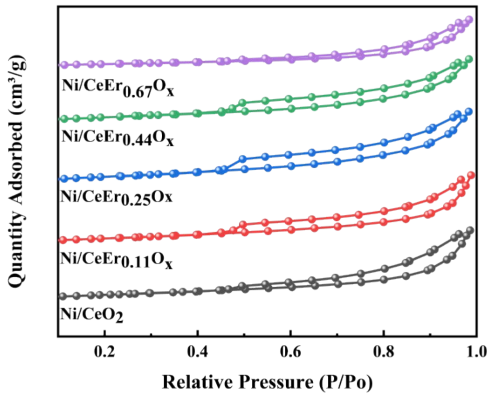

Figure S2. N_2 adsorption–desorption isotherms of catalysts with different Er contents.

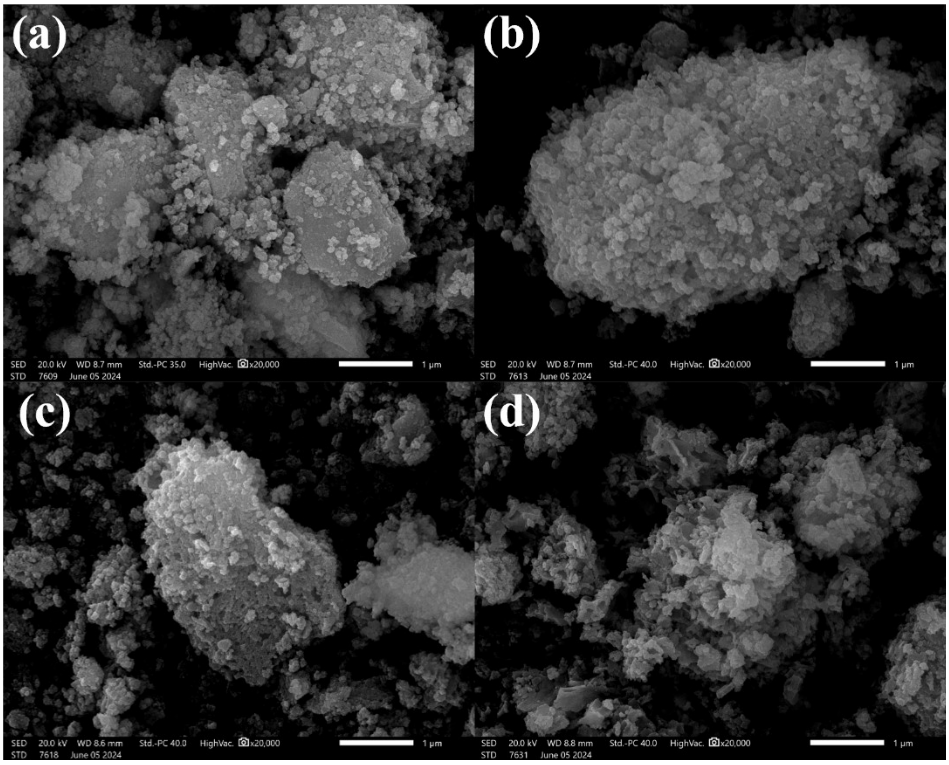

Figure S3. SEM images of catalysts with different Er doping levels: (a) Ni/CeO_2; (b) Ni/$CeEr_{0.11}O_x$; (c) Ni/$CeEr_{0.25}O_x$; (d) Ni/$CeEr_{0.67}O_x$.

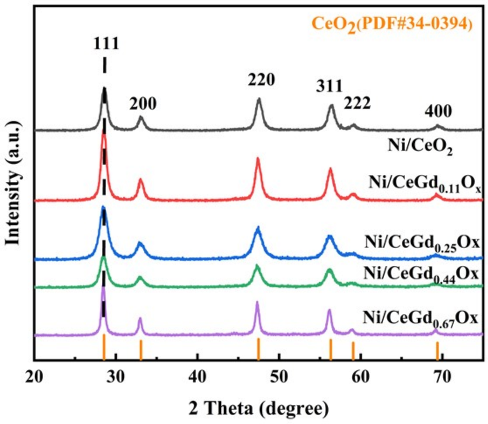

Figure S4. XRD spectra of Gd doped CeO_2.

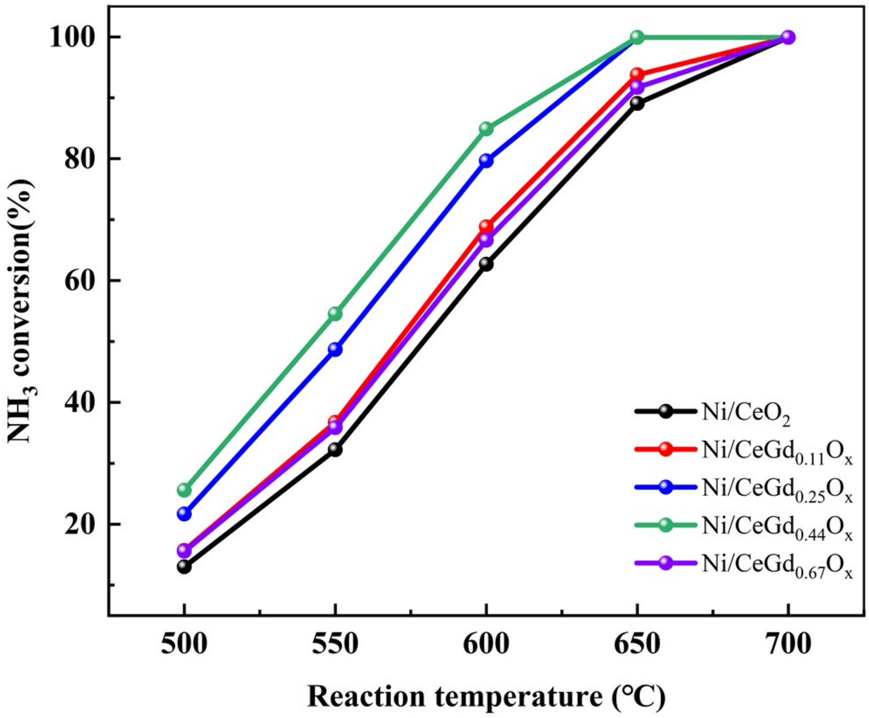

Figure S5. Catalytic performance of Ni/CeO_2 and Gd-doped catalysts with different Gd contents;

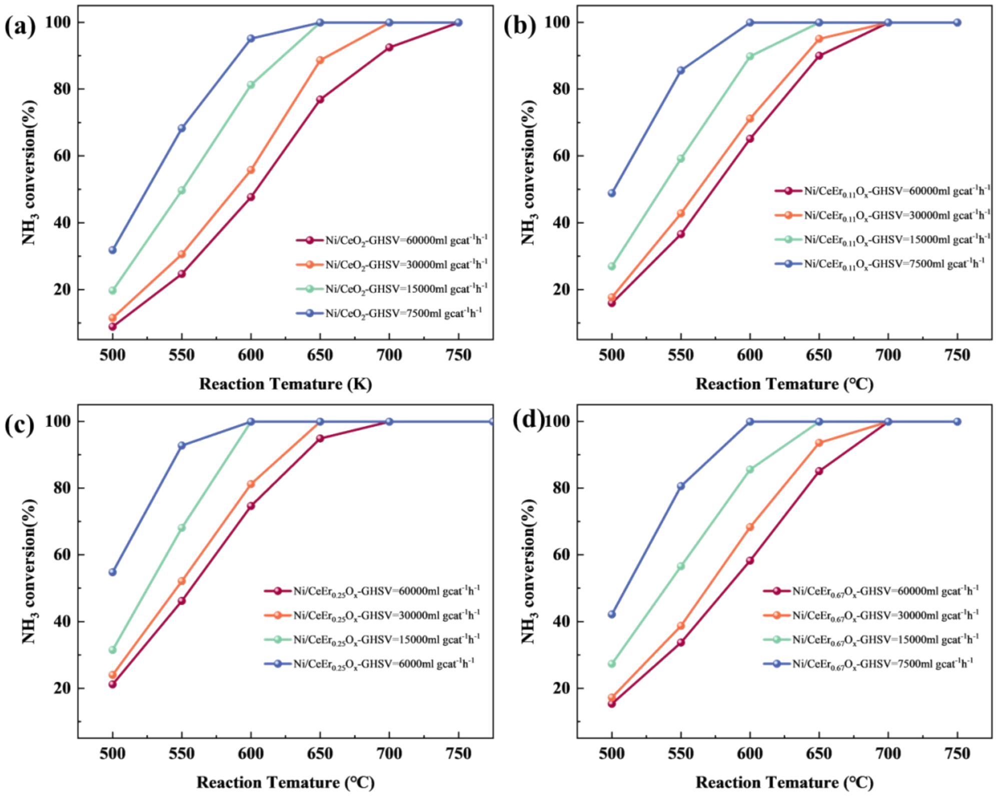

Figure S6. Catalytic activity of catalysts with different Er doping levels: (a) Ni/CeO_2; (b) Ni/$CeEr_{0.11}O_x$; (c) Ni/$CeEr_{0.25}O_x$; (d) Ni/$CeEr_{0.67}O_x$.

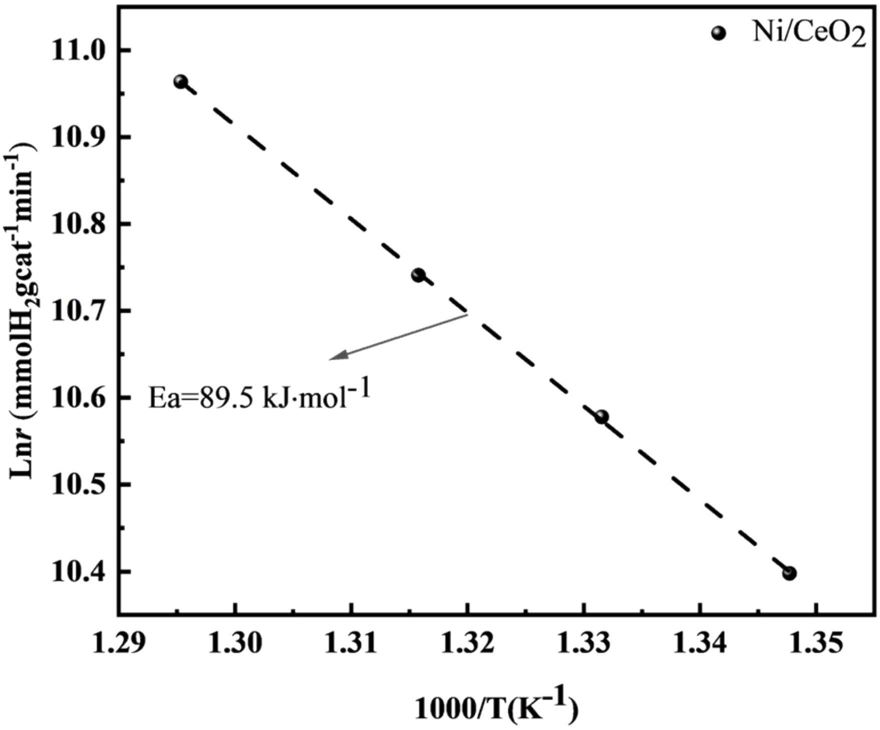

Figure S7. Arrhenius plots for apparent activation energy determination of Ni/CeO_2.

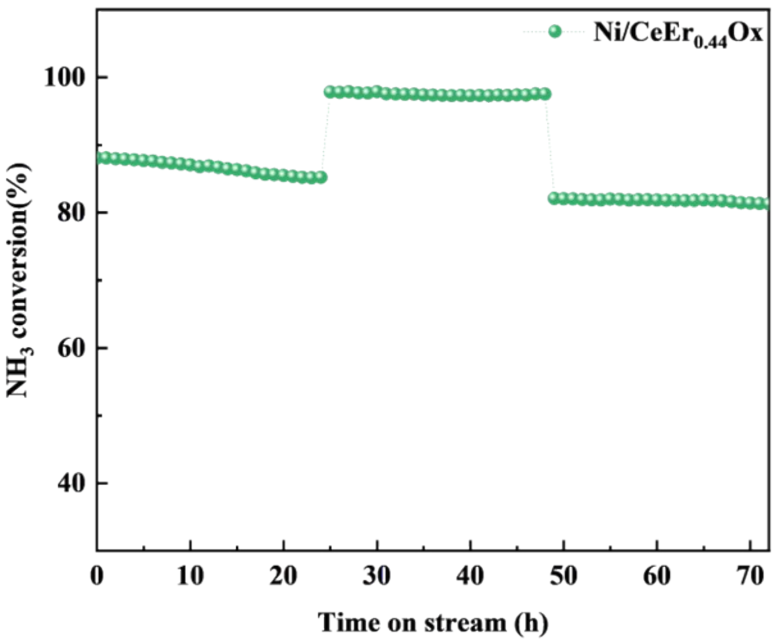

Figure S8. Long-term stability test of Ni/$CeEr_{0.44}O_x$.

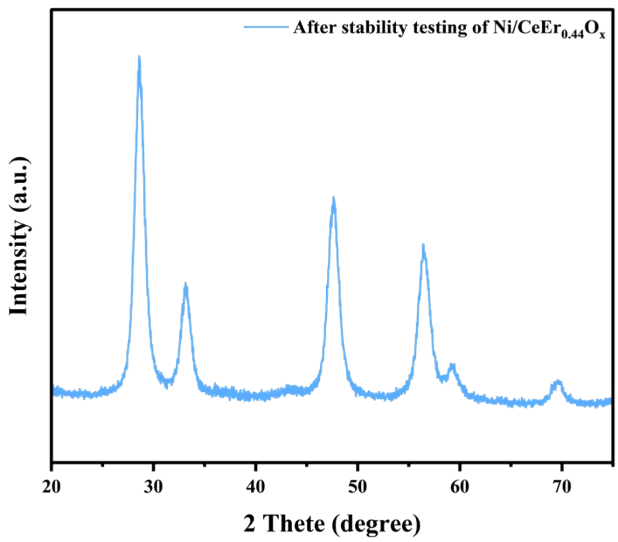

Figure S9. Ni/$CeEr_{0.44}O_x$ XRD pattern after stability testing.

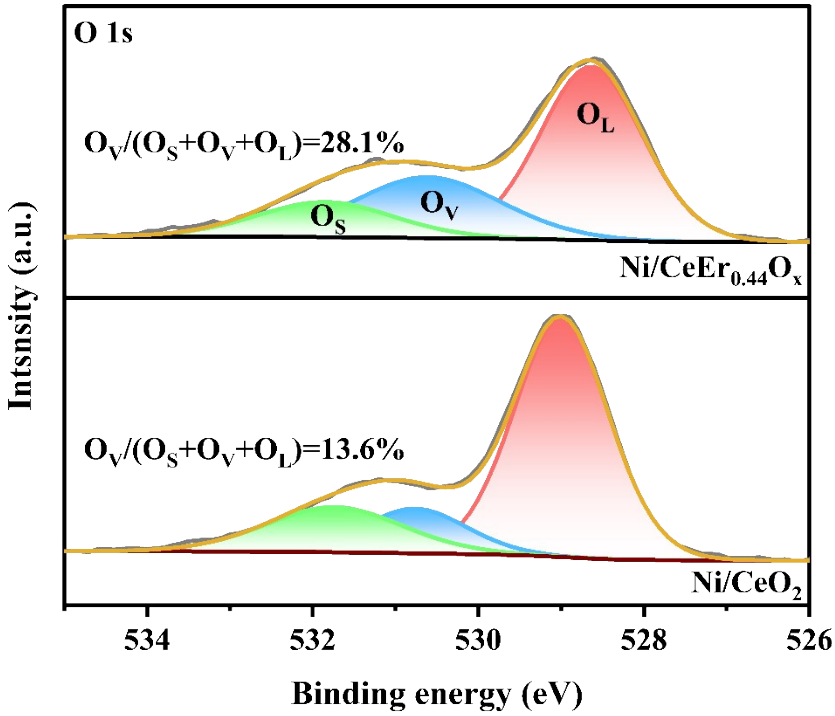

Figure S10. XPS fitting results of O 1s.

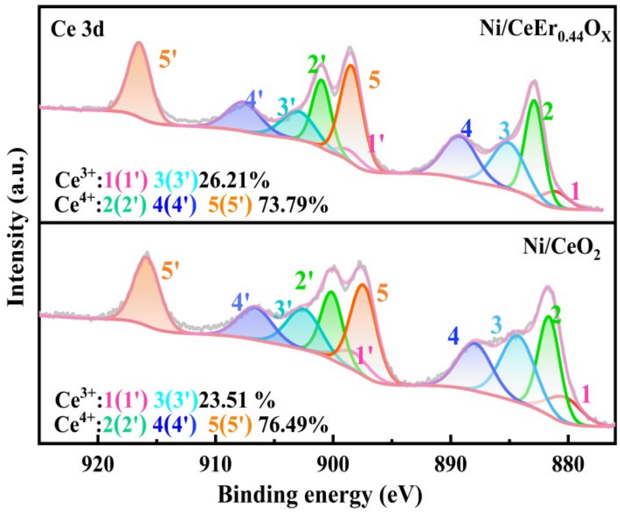

Figure S11. XPS fitting results of Ce 3d.

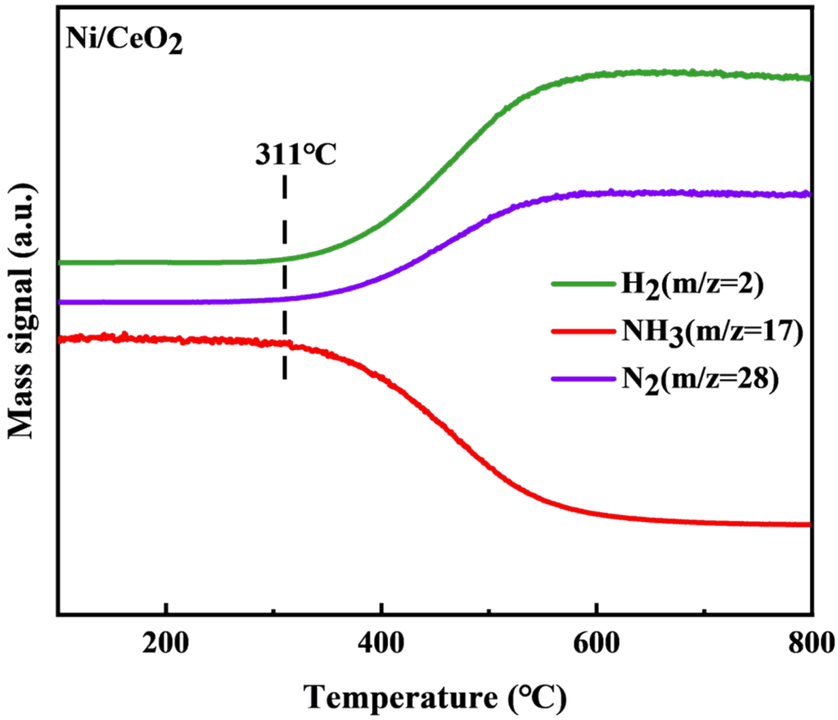

Figure S12. NH_3-TPSR profile of Ni/CeO_2.

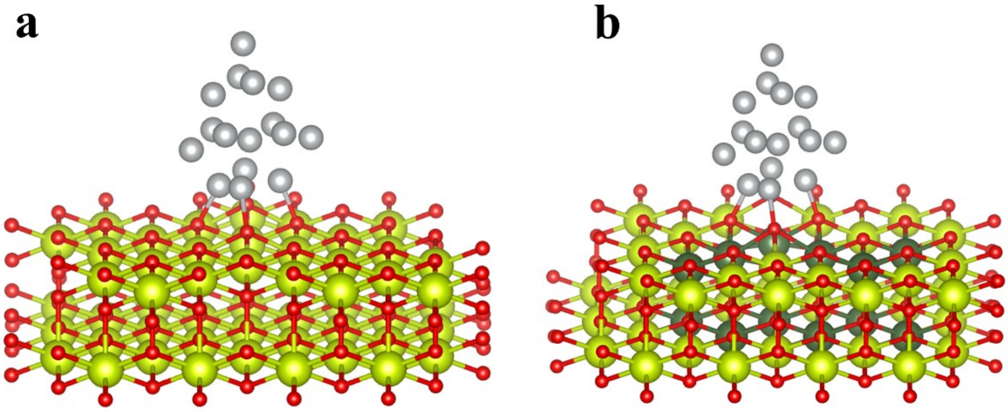

Figure S13. Structural models of Ni/CeO_2 and Ni/$CeEr_{0.44}O_x$.

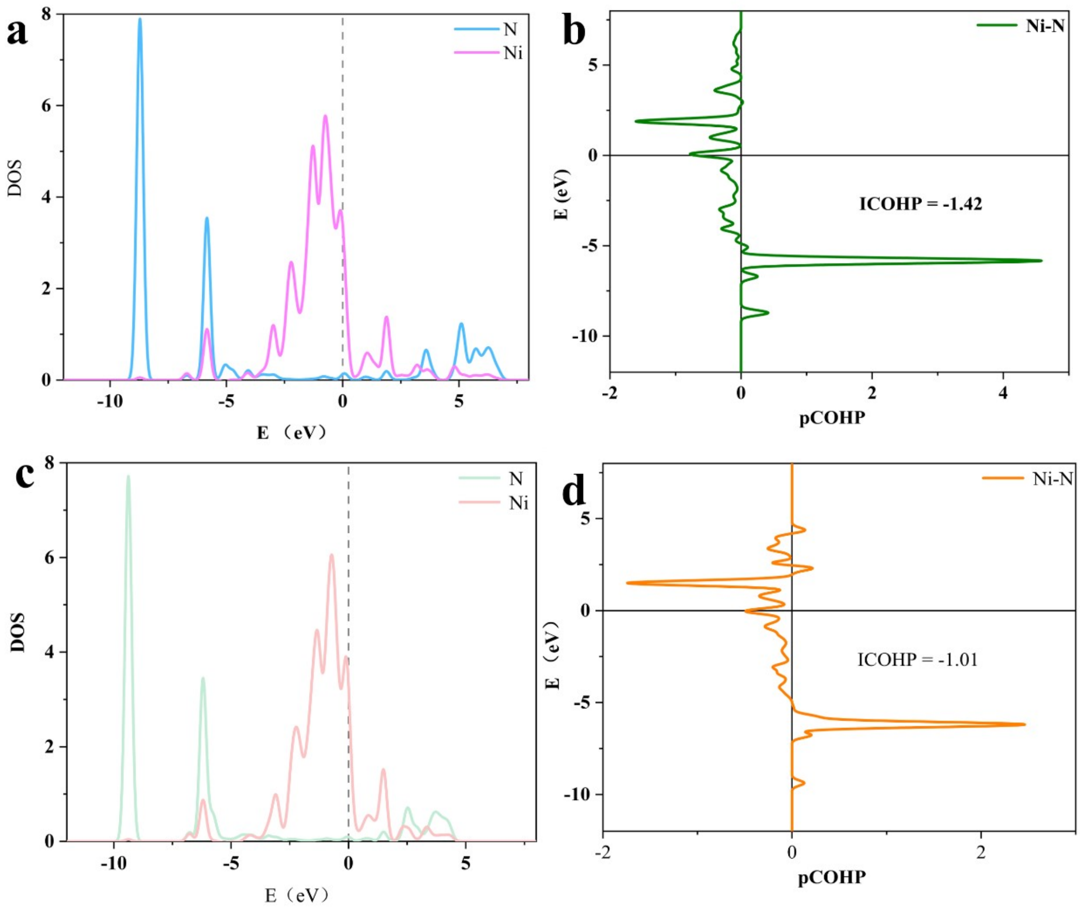

Figure S14. (a) DOS of Ni/$CeEr_{0.44}O_x$; (b) ICOHP of Ni/$CeEr_{0.44}O_x$; (c) DOS of Ni/CeO_2; (d) ICOHP of Ni/CeO_2 for the NH_3 adsorption process.

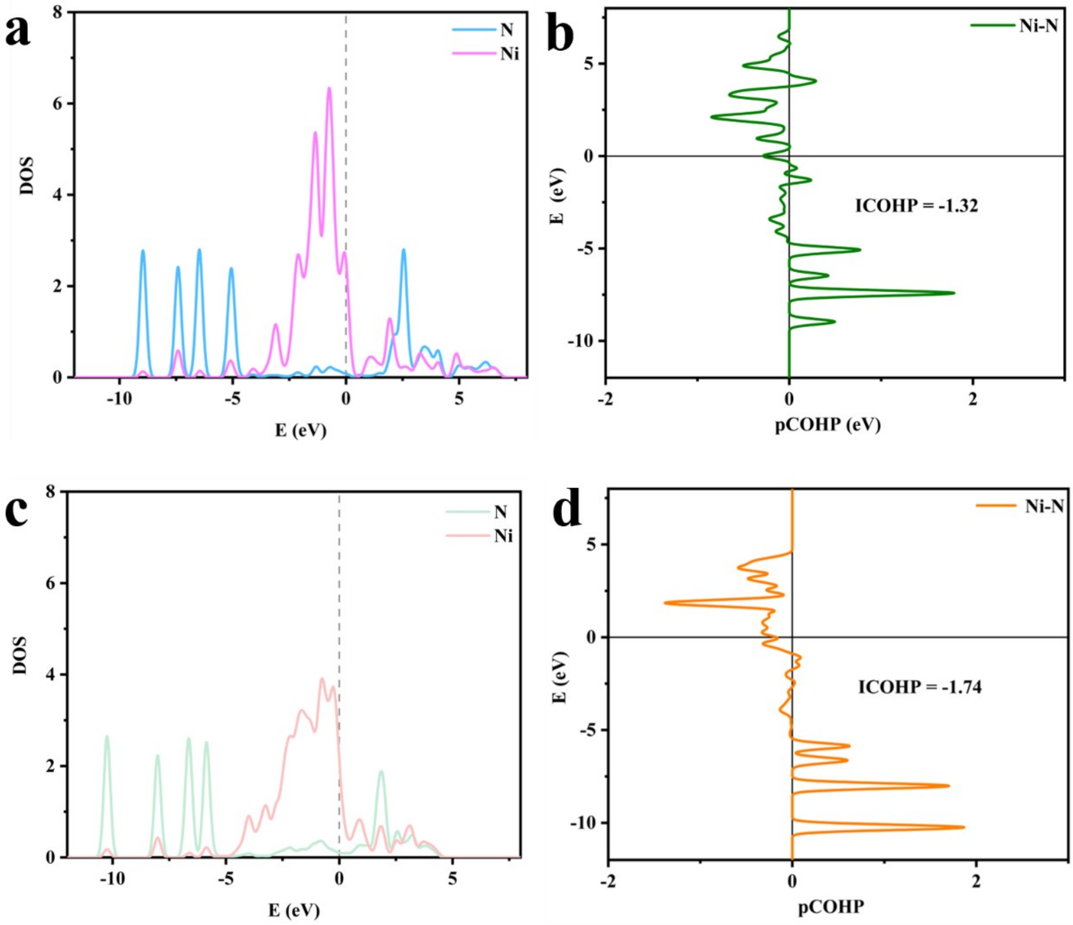

Figure S15. (a) DOS of Ni/$CeEr_{0.44}O_x$; (b) ICOHP of Ni/$CeEr_{0.44}O_x$; (c) DOS of Ni/CeO_2; (d) ICOHP of Ni/CeO_2 for the N–N recombination process.

Table S1. Physicochemical properties of various catalysts.

Catalysts	Surface area ($m^2 \cdot g^{-1}$) [a]	Pore Volumea ($cm^3 \cdot g^{-1}$) [a]	Pore diametera (nm) [a]	Ce contentc (wt.%) [b]	Ni content (wt.%) [b]	Ni dispersion (%) [c]	TOF (S^{-1})
Ni/CeO_2	22.83	0.10	3.08	73.66	7.30	3.72	1.05
$Ni/CeEr_{0.44}O_x$	43.53	0.14	3.13	51.11	5.88	3.33	2.95

a. The textural properties of catalyst were assessed using nitrogen adsorption desorption isothermal measurements. The surface area was determined by the BET equation. Additionally, the pore volume and pore diameter were derived from the BJH adsorption data.

b. The Ni and Ce content of the catalyst was determined based on ICP results.

c. Determined by H_2-pulse chemisorption experiment.

Table S2. Ce–O coordination parameters derived from Ce K-edge EXAFS data.

Sample	Shell	CN[a]	R(Å)[b]	σ^2(10^{-3}Å^2)[c]	ΔE0(eV)	R-factor(10^{-2})[d]
Ni/CeO_2	Ce-O	8.0	2.31	8	4.69	1.7
Ni/$CeEr_{0.44}O_x$	Ce-O	6.9	2.32	4	5.23	0.8

a. CN = coordination number;

b. R = distance between absorber and backscatter atoms;

c. σ^2 = Debye-Waller factor;

d. R-factor indicates the goodness of the fit.